New PVLAS results and limits on magnetically induced optical rotation and ellipticity in vacuum

E. Zavattini[*,1] G. Zavattini,[2] G. Raiteri,[1] G. Ruoso,[3] E. Polacco,[4]

E. Milotti,[1] V. Lozza,[1] M. Karuza,[1] U. Gastaldi,[3] G. Di Domenico,[2]

F. Della Valle,[1] R. Cimino,[5] S. Carusotto,[4] G. Cantatore,[1] and M. Bregant[1]

(PVLAS Collaboration)

[1]*INFN, sezione di Trieste and Dipartimento di Fisica, Università di Trieste*

[2]*INFN, Sezione di Ferrara and Dipartimento di Fisica, Università di Ferrara*

[3]*INFN, Laboratori Nazionali di Legnaro,*

viale dell'Università 2, 35020 Legnaro

[4]*INFN, Sezione di Pisa and Dipartimento di Fisica, Università di Pisa*

[5]*INFN, Laboratori Nazionali di Frascati*

(Dated: June 23, 2007)

---

arXiv:0706.3419v1 [hep-ex] 23 Jun 2007

Abstract

In 2006 the PVLAS collaboration reported the observation of an optical rotation generated in vacuum by a magnetic field. To further check against possible instrumental artifacts several upgrades to the PVLAS apparatus have been made during the last year. Two data taking runs, at the wavelength of 1064 nm, have been performed in the new configuration with magnetic field strengths of 2.3 T and 5.5 T. The 2.3 T field was chosen to avoid stray fields. The new observations do not show the presence of a rotation signal down to the levels of $1.2 \cdot 10^{-8}$ rad @ 5.5 T and $1.0 \cdot 10^{-8}$ rad @ 2.3 T (at 95% c.l.) with 45000 passes. In the same conditions no ellipticity signal was detected down to $1.4 \cdot 10^{-8}$ @ 2.3 T (at 95% c.l.) whereas at 5.5 T a signal is still present. The physical nature of this ellipticity as due to an effect depending on B^2 can be excluded by the measurement at 2.3 T. These new results completely exclude our previously published magnetically induced vacuum dichroism results indicating that they were not of physical origin. These new results therefore also exclude the particle interpretation of the previous PVLAS results. Furthermore the background ellipticity at 2.3 T can be used to determine a limit on the total photon-photon scattering cross section of $\sigma_{\gamma\gamma} < 6 \cdot 10^{-34}$ barn at 95% c.l..

PACS numbers: 12.20.Fv, 07.60.Fs, 14.80.Mz

I. INTRODUCTION

Non linear effects in electromagnetic processes in vacuum have been sought after for many years after having been predicted by Euler and Heisenberg in their effective Lagrangian published in 1936 [1]. The only input to their calculation was the Heisenberg uncertainty principle leading to virtual pair creation, which allowed photons to interact. The direct measurement of this effect is yet to be seen and has been the aim of the PVLAS experiment since its beginnings. The PVLAS experiment, financed by the italian Istituto Nazionale di Fisica Nucleare (INFN), consists of a sensitive ellipsometer attempting to detect the small changes in the polarization state of light propagating through a 1 m long magnetic field region in vacuum. It is based on a high finesse Fabry-Pérot cavity and a superconducting 5.5 T rotating magnet. The experimental setup is located at the Laboratori Nazionali di Legnaro of INFN, Padova, Italy. Indeed vacuum will become birefringent in the presence of a strong magnetic field [2, 3]. A possibile secondary effect, which could mask the vacuum magnetic birefringence, could be due to the existence of a light neutral pseudoscalar/scalar particle coupling to two photons via the Primakov effect [4, 5, 6, 7]. During a number of data taking campaigns from 2000 to 2005, the PVLAS collaboration systematically observed both an induced ellipticity and a rotation of the polarization plane of an initially linearly polarized laser beam after having traversed a 5.5 T magnetic field in vacuum [8]. These observations were in strong contradiction with the Euler-Heisenberg effective Lagrangian predictions in that the observed ellipticity was about 10^4 times greater than expected and, most importantly, a rotation was observed which was not predicted. If one interpreted the observations as due to the existence of a light, neutral, spin-0 boson, and using the results previously obtained by the BFRT experiment [9] the values for mass and inverse coupling of $m = 1$ meV and $M = 4 \cdot 10^5$ GeV, respectively, are found. These values, however, are in strong contradiction with the results from the CAST experiment [10] and with other astrophysical bounds [11]. Many theoretical papers attempting to reconcile the CAST and PVLAS observations were published [12] and several "photon-regeneration" experiments were started [13, 14] to try to directly detect the particle candidate in an appearance experiment rather than a disappearance one, as it is the case in PVLAS experiment. The published PVLAS rotation results regarded an empirical finding which was attributed to an effect originating in the Fabry-Pérot cavity with the magnetic field energized. The origin of this signal, whether

physical or instrumental, was unknown, however the diagnostic tests originally performed allowed us to localize the effect in the cavity and to exclude several spurious signal sources, such as those due to electromagnetic pick-ups or to a direct action of the fringe fields on the optical components. In fact, given that it was not possible to completely eliminate them, the fringe fields remained a plausible source of instrumental artifacts, albeit in conjunction with some yet to be found indirect effect. After several apparatus upgrades designed to minimize the effect of the fringe fields, which we discuss below, we carried out several measurement runs both at the maximum field strength of 5.5 T and at the reduced field intensity of 2.3 T, when no measurable stray field is present. The results from these measurements do not confirm the presence of a rotation signal at the expected frequency, also excluding the presence of an ellipticity signal at 2.3 T. We discuss below the details of these measurements. The background ellipticity and rotation values can be used to establish upper bounds on the total photon-photon scattering cross section (ellipticity) and to set an exclusion zone in the mass-inverse coupling parameter plane for scalar/pseudoscalar bosons coupled to two photons.

II.   APPARATUS AND EXPERIMENTAL TECHNIQUE

Figure 1 shows a schematic layout of the PVLAS apparatus. The 1 m long interaction region is contained within a 4.6 m long, 25 mm diameter quartz tube. This tube is placed vertically and traverses the bore of the dipole magnet. The magnet is housed within a 5 ton, 3.1 m high, warmbore cryostat, and the field direction lies in the horizontal plane: the cryostat itself sits on a 0.9 m radius turntable standing on a concrete beam fastened to the experimental hall floor. The UHV vacuum chambers hosting the optical elements, placed at the top and at the bottom of the tube, are fastened to two granite optical benches. These benches are fixed on a concrete platform mechanically isolated from the rest of the hall floor. During normal operation the cryostat is filled with liquid He at 4.2 K and the magnet is energized with a current of about 2030 A, resulting in a 5.5 T field over the entire interaction region. To allow rotation of the magnet, the coils are shorted and disconnected from the power supply. The field intensity is monitored by a set of Hall probes [8]. The turntable is actuated by a low-vibration hydraulic drive and normally rotates the magnet-cryostat assembly, around a vertical axis, at a frequency $\Omega_{mag} \approx 0.3$ Hz. During vacuum measure-
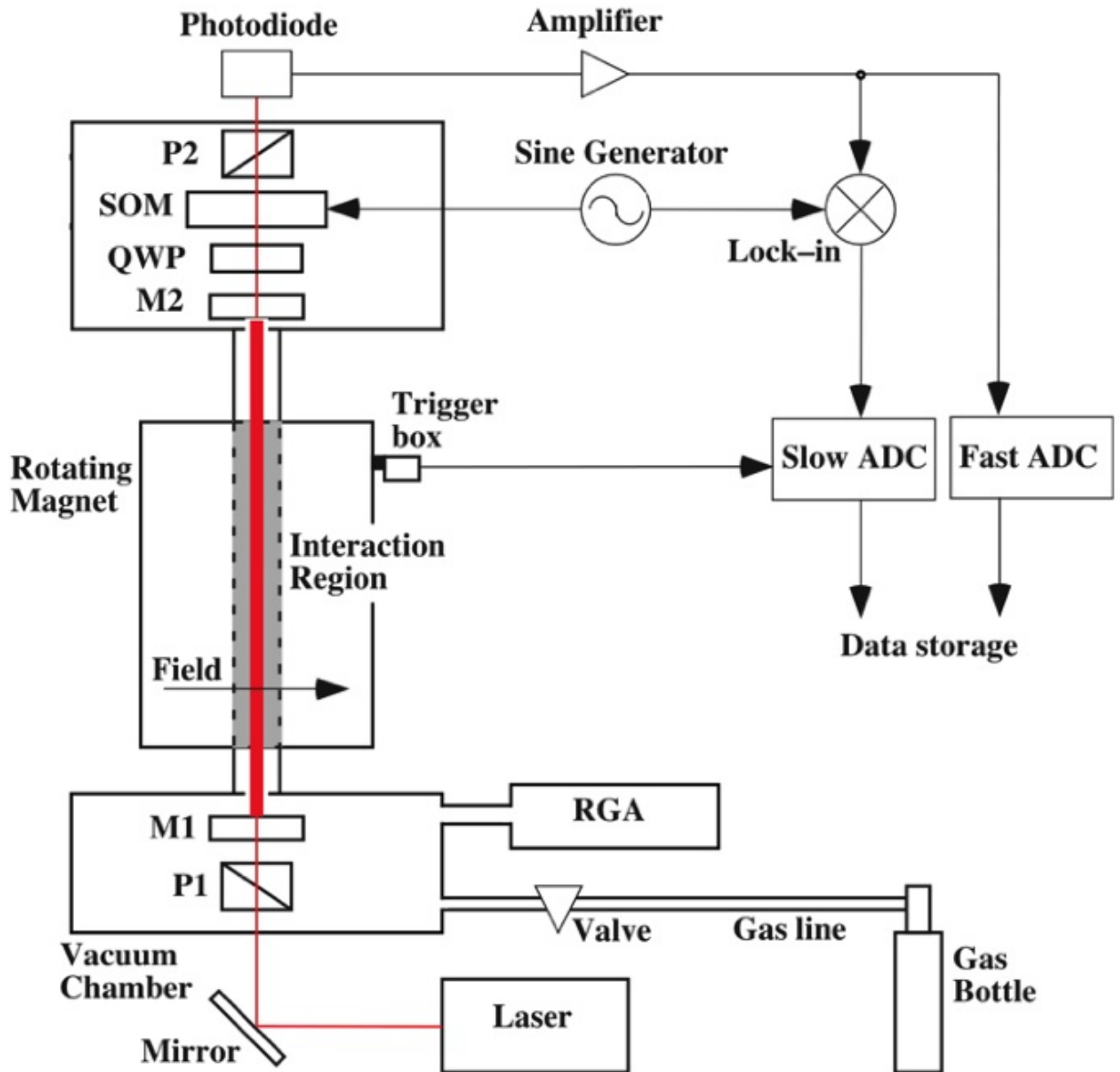
Figure 1: *Schematic layout of the PVLAS apparatus. See text for description.*

ments, the quartz tube and the two vacuum chambers are kept in UHV conditions ($P \approx 10^{-8}$ mbar) by two liquid N_2 traps combined with Ti sublimation pumps. This pumping scheme has been chosen in order to avoid mechanical vibrations and possible couplings between the rotating dipole field and the ion-pump permanent magnets. The residual gas composition is monitored by means of a residual gas analyzer (RGA). The interaction region, where

the 1064 nm laser beam propagates, is contained within a high-finesse Fabry-Perot optical resonator (FP) formed by a pair of dielectric, multilayer, high reflectivity, 11 m curvature radius mirrors placed 6.4 m apart (M1 and M2). Resonator diffraction losses are found to be negligible. The ellipsometer consists of a pair of crossed polarizing prisms (P1 and P2) together with an ellipticity modulator, a stress optic modulator (SOM)[15]. A quarter wave plate can be inserted between the upper cavity mirror M2 and the ellipticity modulator SOM in order to be sensitive to rotations generated within the FP cavity.

III. METHOD

In the PVLAS apparatus signals are detected by measuring the light intensity transmitted by the analyzer P2, crossed with P1. An electric field component perpendicular to the entrance polarization fixed by the polarizer P1 may be generated within the FP cavity if an ellipticity ψ is induced by a birefringence or a rotation α is induced by a Faraday effect or a dichroism. A rotation due to the Faraday effect (circular birefringence) is parametrized by the Verdet constant and is linear in the magnetic field intensity B. Such a rotation is induced by a magnetic field component parallel to the beam propagation. A dichroism, or differential absorption of different polarizations, can be described by the difference in linear absorption coefficient $\Delta\kappa$ of the medium for two orthogonal polarizations. Similarly, a linear birefringence can be described as the difference Δn between the indices of refraction for two polarizations, one parallel to some optic axis (in our case the magnetic field) of the medium, and the other one normal to it. Given a path length L, a birefringence Δn and a dichroism $\Delta\kappa$, these will generate respectively an ellipticity ψ and rotation α

$$\psi = \frac{\pi\Delta nL}{\lambda}\sin 2\vartheta \tag{1}$$

$$\alpha = \frac{\Delta\kappa L}{2}\sin 2\vartheta \tag{2}$$

In the case of a magnetically induced birefringence or dichroism, it is important to note the dependence of both the ellipticity and rotation, respectively, on twice the angle ϑ between the polarization and the magnetic field.

A phase difference of $\pi/2$ between an ellipticity and a rotation allows one to distinguish the two effects. In fact if $\eta(t)$ is the ellipticity induced by the SOM and the quarter wave

plate is out of the beam path, the intensity I_{tr} transmitted by the analyzer P2 will be

$$I_{tr} = \left|E_A\right|^2 = I_0 \left[\sigma^2 + \left|\alpha(t) + \imath\eta(t) + \imath\psi(t)\right|^2\right]$$
$$\simeq I_0 \left[\sigma^2 + \left(\eta(t)^2 + \alpha(t)^2 + 2\psi(t)\eta(t) + \psi(t)^2\right)\right] \tag{3}$$

where we have also introduced the extinction ratio of the polarizers σ^2. The imaginary nature of the electric field component due to the ellipticities $\psi(t)$ and $\eta(t)$ compared to the real nature of rotations is explicitly shown. The result is that only ellipticities will be linearized and will therefore beat with the SOM.

Therefore, if the magnet rotation is at the angular frequency Ω_{Mag} and the SOM is modulated at the angular frequency ω_{SOM}, a physical signal generated by a magnetically induced linear birefringence will generate a Fourier component at $\omega_{SOM} \pm 2\Omega_{Mag}$. Static ellipticities present are contained in the $\imath\psi(t)$ term of Eqn. (3) and can be compensated by acting directly on the SOM itself by a dedicated PZT.[15]

With the quarter wave plate inserted the roles of $\psi(t)$ and $\alpha(t)$ will be inverted.[16] Furthermore, the quarter wave plate may be used in two different orientations by simply exchanging the slow and fast axes. In fact, a real component (rotation) $\alpha(t)$ will become an imaginary one with its sign depending on the QWP orientation. The vector difference of signals measured with the two QWP orientations will isolate effects generated before the QWP. This, in conjunction with the fact that one does not observe signals above background with the FP cavity removed, allows one to further narrow down the source of measured rotation or birefringence effects to the cavity alone.

IV. EARLY OBSERVATIONS

A. Previously published results and relative diagnostic tests

The results of the rotation measurement from the first series of data taking runs done with the PVLAS apparatus were published in [8]. In this work, we reported the observation of a rotation peak at the frequency $\omega_{SOM}\pm2\Omega_{Mag}$ with an amplitude of $(3.9\pm0.5)\cdot10^{-12}$ rad/pass, corresponding to $(1.7\pm0.2)\cdot10^{-7}$ rad when 44000 passes are considered. The peak appeared with the magnet energized at 5.5 T and the FP cavity present. Its phase, after an averaging procedure, was found to be compatible with the phase expected from a physical signal.

Similar results, albeit with a less clear signature, were found for ellipticity measurements, yielding an average value of $\approx 2 \cdot 10^{-7}$ for 44000 passes at 5.5 T. The ellipticity data are, however, unpublished. A first series of diagnostic tests was conducted on these rotation and ellipticity signals with the aim to investigate their nature, physical or instrumental. Focus was placed on proving/disproving the fact that the observed peaks were "optical", meaning that they were present in the spectrum of the detection photodiode current as a consequence of changes of the polarization state of the light propagation through the apparatus. For instance, attention was put on checking whether signal peaks could be due or not to a simple electromagnetic pick-up. A list summarizing the considered sources of instrumental artifacts, together with corresponding experimental tests, is given in Tables I and II below.

B. Fringe field effects

Fringe fields acting on the different optical elements may generate components of both $\psi(t)$ and $\alpha(t)$. These direct optical effects were verified not to induce significant instrumental artifacts at twice the rotation frequency of the magnet. The Faraday rotation for the various elements (polarizers, SOM, mirrors and QWP) was measured directly, including the reflective surface of the mirrors. The measured Verdet constants for our mirrors at 1064 nm are $(6.4 \pm 1.0) \cdot 10^{-1}$ rad/T/m for the mirror substrate (fused silica, thickness $8 \cdot 10^{-3}$ m), and $2 \cdot 10^{-7}$ rad/T/reflection for the multilayer high-reflectivity coating. This last number compares well with the results found in [17]. When operating at 5.5 T the measured vertical stray field component is about 10^{-4} T at Ω_{Mag} and of about 10^{-7} T at $2\Omega_{Mag}$. One therefore finds a contribution to the rotation signal amplitude of $1.4 \cdot 10^{-6}$ rad at Ω_{Mag} and of $1.9 \cdot 10^{-9}$ at $2\Omega_{Mag}$ (a finesse of 70000 was considered and the presence of both mirrors has been taken into account). It is clear, then, that the typical amplitude of the Ω_{Mag} rotation signal ($\approx 2 - 3 \cdot 10^{-6}$) is practically entirely due to a fringe field induced Faraday effect, while the contribution at $2\Omega_{Mag}$ is below the observed rotation background. In fact, when Helmholtz coils placed around the FP cavity mirrors (see below) are used in feedback mode to cancel all the stray field components including the vertical one, the Ω_{Mag} signal peak is strongly suppressed. The missing suppression factor can be explained by the fact that the field sensor necessary for the feedback loop is not placed in the exact mirror position, rather, it is fixed at

Table I: List of instrumental artifacts which could account for the early observations of rotation [8] and birefringence signals. All these sources of artifacts were excluded (see also text).

Origin	Test	Comment
Magnetic rotation/ellipticity from a residual gas	Measure the pressure and composition of the residual gas.	No polarization rotation is generated by gases in a magnetic field perpendicular to the propagation direction. A birefringence is generated by the Cotton-Mouton effect, however the Cotton-Mouton effect due to the worst contaminant is orders of magnitude below the observed effect.
Rotation/ellipticity induced by fringe fields on the mirror coatings	Direct measurement of the effect.	Magnetically induced rotation and birefringence effects due to fringe fields acting parallel and normal to the mirror surface have been directly measured. Their magnitude cannot account for the observed peaks (see discussion in the text).
Electronic pick-up (rotation and ellipticity)	Measure with field ON and the cavity mirrors removed.	Pick-up is excluded at the level of $\approx 2 \cdot 10^{-8}$ (ellipticity and rotation).

a horizontal distance of about 10 cm. With respect to the horizontal stray field components, measured to be ≈ 2.5 G at Ω_{Mag} and of $\approx 10^{-2}$ G at $2\Omega_{Mag}$, when using the result reported in [18], giving an induced birefringence of $\approx 10^{-17}$ rad/G^2/reflection, one finds a negligible contribution to the birefringence at $2\Omega_{Mag}$ of $\approx 6 \cdot 10^{-12}$. The absence of an effect on the mirrors due to a horizontal field was also verified directly with the Helmholtz coils. Eventually, after a series of tests such as those described in Tables I and II, the suspected source of instrumental artifacts was narrowed down as due to the stray field generated by the superconducting magnet. The action of this field must however be indirect, meaning that it must couple to some other instrumental effect in order to account for the following

Table II: Table I continued

Origin	Test	Comment
Diffused light from a magnetized inner surface of the cryostat bore (birefringence)	Change the geometrical acceptance of the light detection system.	A spatial filter is present before the detection photodiode. Data taken with several different pinhole diameters down to $50\,\mu$m showed no change in the observed signal.
Field-induced movement of the polarizer and/or the QWP (rotation)	Measure with field ON and the cavity mirrors removed.	Excluded by measurements with field on and cavity mirrors removed (see comment on pick-ups in Table I)
Spurious, field-induced ellipticity generated by the SOM modulator	Measure with the field ON and the cavity mirrors removed	Excluded by measurements with field on and cavity mirrors removed (see comment on pick-ups in Table I)
Unknown field-polarization coupling	Eliminate the fringe fields.	This coupling cannot come from a *direct* effect of the fringe fields. However, and *indirect* effect, meaning a conspiracy of more than one instrumental artifact, cannot be excluded by the above tests

empirical findings on the nature of the signal peaks (rotation and ellipticity): the effect is due to the presence of the FP cavity, it changes sign following a change in the orientation of the QWP (rotation) or of the SOM (ellipticity), there is no measurable direct effect of the stray fields on the cavity mirrors and on the other optical elements.

C. Apparatus upgrades

With the main intent of reducing the supposed effects of the fringe fields several upgrades were made to the setup. A new He gas compressor was installed, increasing the overall

efficiency of the magnet cooling cycle and resulting in longer running periods at 4.2 K. We changed the laser, going from a Nd:YAG laser at 1064 nm made by Lightwave Inc., to a laser based on the same active crystal made by Innolight GmbH. The new laser has actually two beam ports, one emitting at 1064 nm with a maximum power of about 800 mW, and a second one emitting a frequency-doubled beam at 532 nm, with a maximum power of about 100 mW. The 1064 nm beam was used in order to compare data directly with the old measurements. The laser head was also shielded with μ-metal, along with the circuitry used in the electo-optic feedback loop necessary to frequency-lock the laser to the cavity. The previous access structure to the optics tower, which was made almost entirely of iron, was substituted with an aluminum one. All coaxial signal cables were replaced with new cables with better shielding. Two sets of three-axis Helmholtz coils, one set around each cavity mirror, were put in place. These allowed both local zeroing of the residual magnetic field and the possibility to actively excite the mirrors with a given field intensity and direction. Finally, the initial fixed linear polarization of the light beam has been rotated by 54° with respect to the previous measurements and is now normal to the beam supporting the rotating magnet.

V.   NEW RESULTS

Gas measurements, for calibration, and vacuum measurements were conducted with the apparatus in the new upgraded configuration. The FP cavity was operating at a typical finesse of 70000. Several diagnostic runs were also done with the Helmholtz coils active or off, in order to test the effect of locally canceling the stray field. When the magnet is energized at 2.3 T, from measurements with field probes, we found that the stray field is about a factor 50 smaller than at 5.5 T. Therefore, in order to globally check against fringe field effects, two measurement campaigns in vacuum were performed with the apparatus in the new upgraded configuration. First both ellipticity and rotation measurements at 2.3 T (no fringe field), then both ellipticity and rotation measurement at 4 T and at the maximum 5.5 T field (fringe fields present). In addition, a series of diagnostic tests was carried out in order to check whether *indirect* instrumental causes could be used to explain the presence/absence of the rotation and birefringence signal peaks.

A. Gas calibration measurements

To verify the correct functioning of the apparatus, calibration measurements were taken with different gases. In the presence of an external magnetic field, a gas will become birefringent due to the Cotton-Mouton effect[19]. These measurements also allow the determination of the the physical phase of the Fourier component at twice the rotation frequency of the magnet, $2\Omega_{Mag}$. Indeed, the ellipticity induced by a birefringence is maximum when the angle between the polarization and the slow axis is 45°. In our apparatus this translates into a phase at $2\Omega_{Mag}$ of 125°. Figure 2 shows a polar plot corresponding to the amplitude and phase of the signal due to Helium gas at 4 different pressures: 5, 10, 15 and 20 mbar. These measurements were taken with a field intensity of 2.3 T. A gas with a negative Cotton-Mouton constant would generate a signal at 180° with respect to the signals shown in Figure 2. Having defined the physical axis, our results will be presented as components parallel and perpendicular to it. A positive component along the physical axis will mean a positive birefringence.

B. Vacuum measurements

A summary of the typical spectra obtained in the measurements presented here is shown in Figure 3. A spectrum, corresponding to about 600 s of data acquisition time, is given for each of the three possible configurations of the apparatus and for three different field intensities. The "no QWP" column shows ellipticity spectra taken with the QWP removed from the beam, and the two columns QWP0 and QWP90 show rotation spectra taken with the QWP in the beam path with two different orientations. The frequency span is chosen in such a way as to show only the higher frequency sidebands of the 506 Hz carrier frequency.

The final results are deduced from the data by taking a vectorial weighted average of 100 s long subdatasets. A Fourier transform of the complete data set, for each configuration, is also taken to have the best frequency resolution in the possible presence of a peak. Indeed due to the in-phase data acquisition, a physical signal should occupy a single bin in such a spectrum.
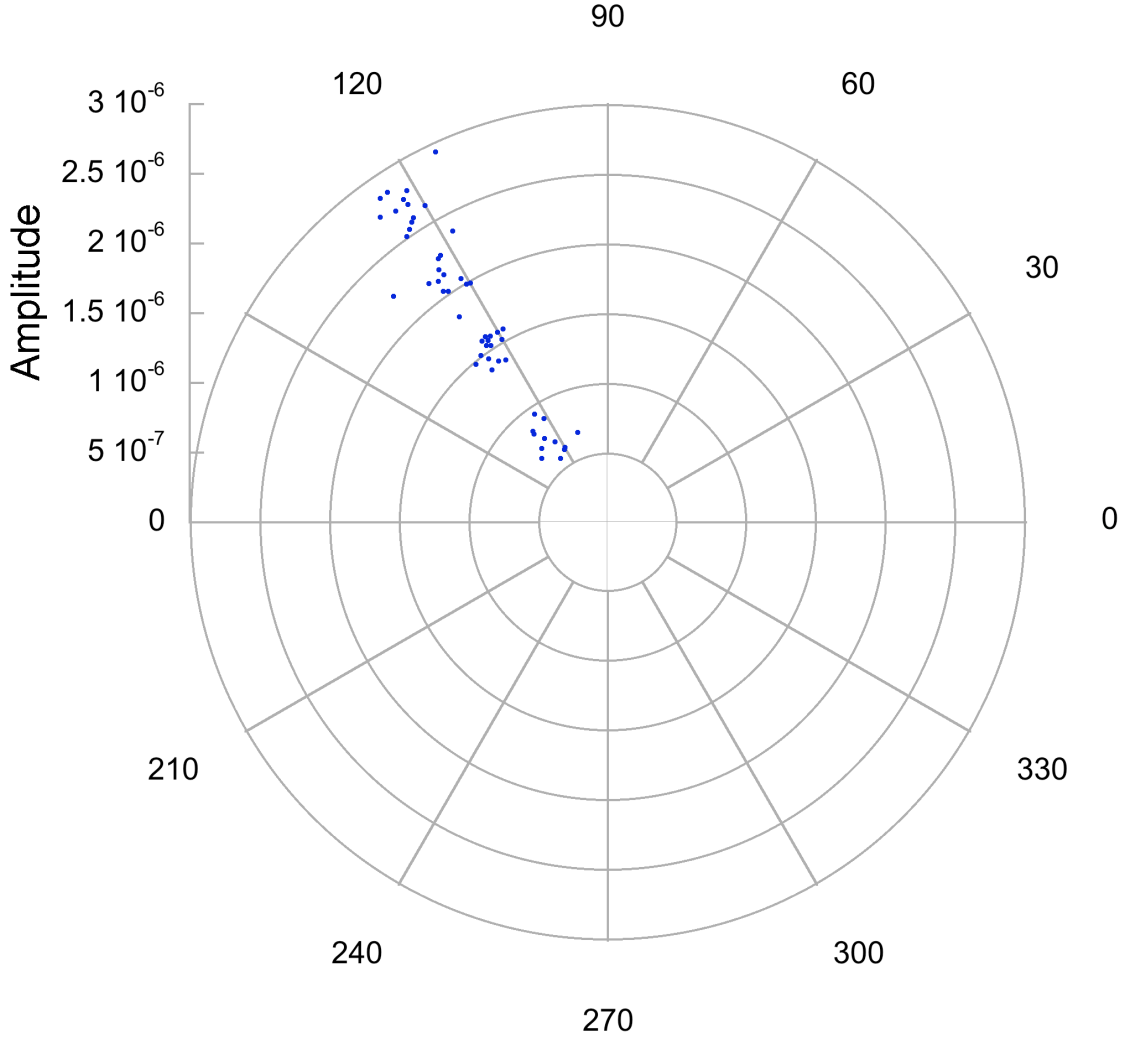
Figure 2: *Polar plot for the ellipticity signal generated with a 2.3 T magnetic field intensity when Helium gas is present in the vacuum chamber. The figure shows the signal for 4 different gas pressures: 5, 10, 15 and 20 mbar. Each data point represents amplitude and phase of the signal peak observed in a 100 s long time record.*

1. *Rotation measurements*

In the rotation columns ("QWP0" and "QWP90"), of Figure 3, no signal peaks appear at twice the magnet rotation frequency at 0 T, 2.3 T, and at 5.5 T. Peaks at twice the magnet rotation frequency remained absent also when the analysis was extended, for a given field intensity, to the entire available data set.

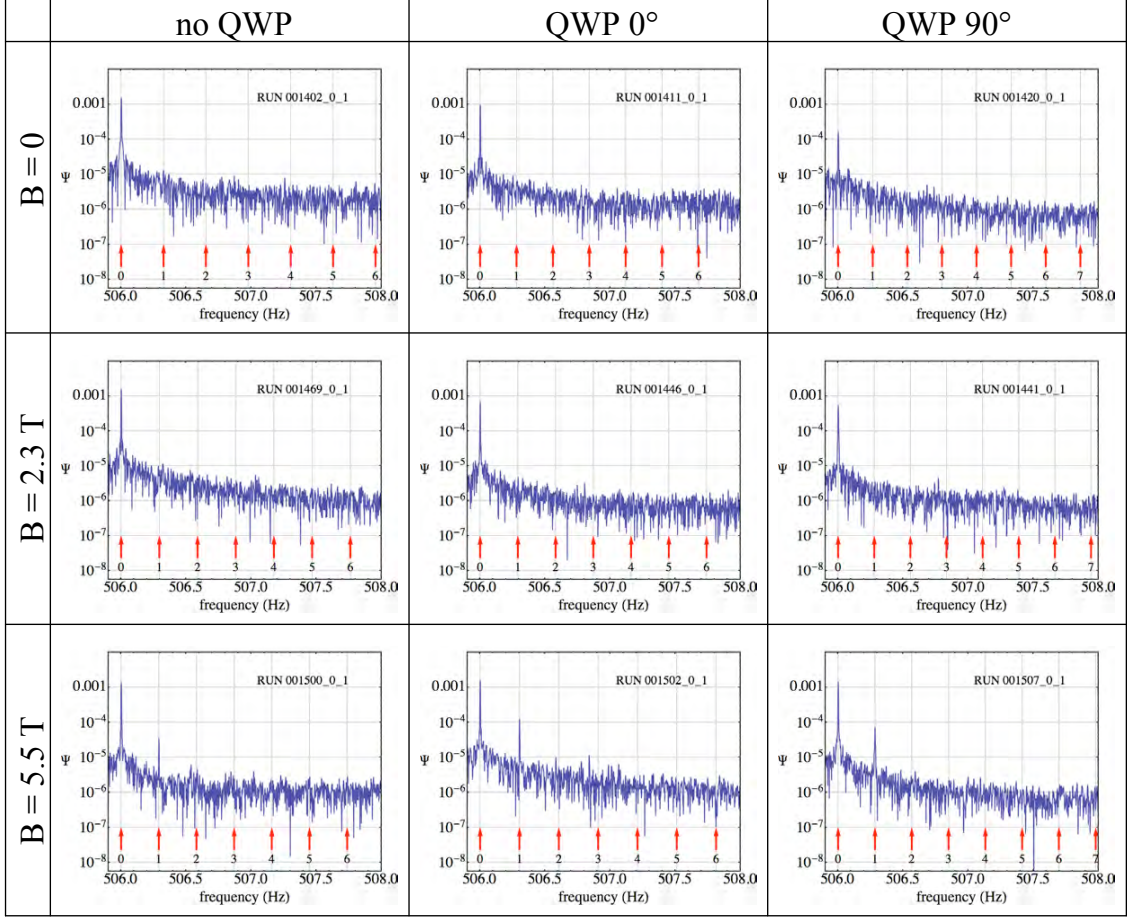Histograms of the noise from the Fourier spectrum, for the 2.3 T data, in the frequency

Figure 3: *Summary table of typical spectra observed in vacuum in the measurements reported here (see text)*

interval $1.92\Omega_{Mag} - 2.08\Omega_{Mag}$, for the QWP0 and QWP90, data are shown in Figure 4 at left. A fit with a Rayleigh probability distribution is superimposed. This is the probability density function which results for the amplitude of a signal having a Gaussian distribution with equal standard deviations, σ, along two orthogonal axes. A vertical line indicates the value obtained from the weighted average of the 100 s subdatasets at $2\Omega_{Mag}$. The components of these vectors projected along the physical axis, PA, and along the orthogonal one, NPA, are

$$QWP0: \quad PA = (-3.5 \pm 6.0) \cdot 10^{-9} \text{ rad}$$
$$NPA = (-2.9 \pm 6.0) \cdot 10^{-9} \text{ rad}$$
$$QWP90: \quad PA = (4.6 \pm 5.9) \cdot 10^{-9} \text{ rad}$$
$$NPA = (-13 \pm 5.9) \cdot 10^{-9} \text{ rad}$$

14

A zoom in the frequency spectrum around $2\Omega_{Mag}$ is also shown in Figure 4 at right. Neither the QWP0 nor the QWP90 histograms present a peak above the noise. From the cumulative Rayleigh probability distribution $(F(x) = 1 - e^{-0.5(\frac{x}{\sigma})^2})$ one can give a limit on the induced rotation at $2\Omega_{Mag}$ of $x_{QWP0} = 1.5 \cdot 10^{-8}$ rad at a 95 % confidence level in the QWP0 configuration, and $x_{QWP90} = 1.4 \cdot 10^{-8}$ rad at a 95 % confidence level in the QWP90 configuration. By taking the weighted vector average between the QWP0 and QWP90 results, taking into account the sign difference in the two measurements, one obtains an amplitude $\Delta_{2.3T} = (6.8 \pm 4.2) \cdot 10^{-9}$ rad well within the 95% confidence limit of $x_{2.3} = 1.0 \cdot 10^{-8}$ rad. The total measurement time at 2.3 T field intensity was 47300 s.
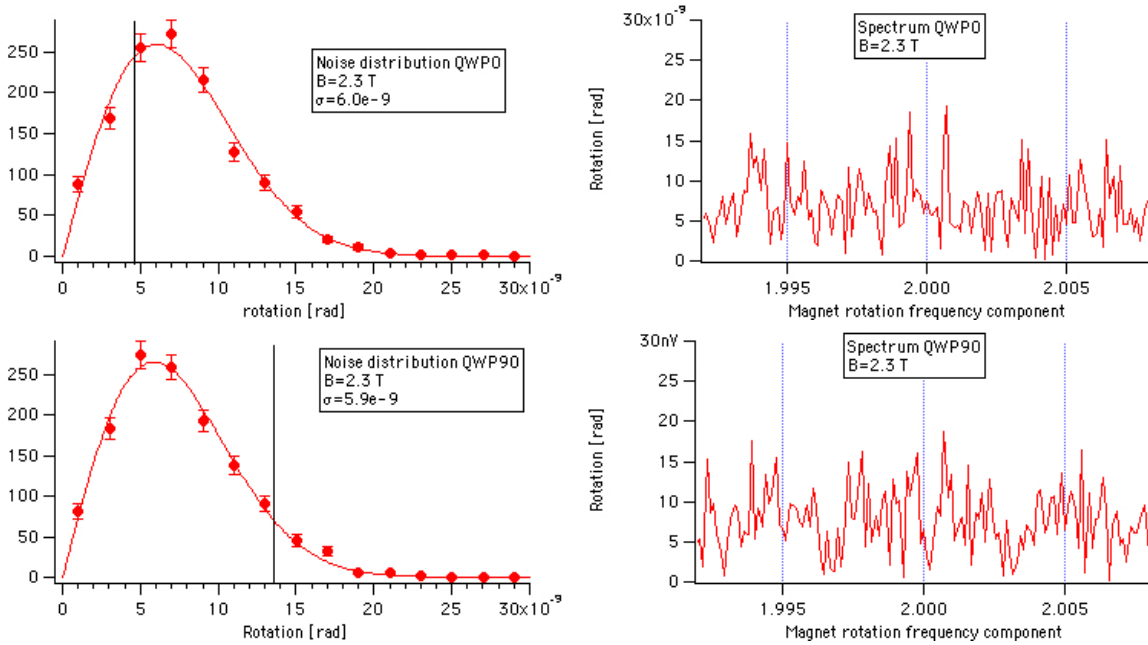

Figure 4: *Left: QWP0 and QWP90 noise distributions in the magnet rotation frequency band* $1.92\Omega_{Mag}$ - $2.08\Omega_{Mag}$ *for the 2.3 T rotation measurements. The vertical line indicates the resulting amplitude determined from a weighted average of 100 s long data subsets. Indicated is the value of σ for the two configurations. Right: zoom around $2\Omega_{Mag}$ of the Fourier spectrum of the entire data set showing no significant peak at the $2\Omega_{Mag}$ (see text).*

The corresponding noise histograms and spectra for the 5.5 T measurements are shown in Figure 5, at left, in the frequency band $1.92\Omega_{Mag}$ - $2.08\Omega_{Mag}$. Again the spectra do not show a definite peak at $2\Omega_{Mag}$. The weighted vector average of the 100 s data subsets results

are

$$QWP0: \quad PA = (2.5 \pm 7.3) \cdot 10^{-9} \text{ rad}$$

$$NPA = (6.2 \pm 7.3) \cdot 10^{-9} \text{ rad}$$

$$QWP90: \quad PA = (2.1 \pm 6.5) \cdot 10^{-9} \text{ rad}$$

$$NPA = (-12 \pm 6.5) \cdot 10^{-9} \text{ rad}$$

The total integration time at 5.5 T was 30100 seconds. By taking a weighted vectorial average, $\Delta = \frac{QWP0 - QWP90}{2}$, one obtains $\Delta_{5.5} = (9.4 \pm 4.9) \cdot 10^{-9}$ again well within the 95% condidence limit of $x_{5.5} = 1.2 \cdot 10^{-8}$ rad.
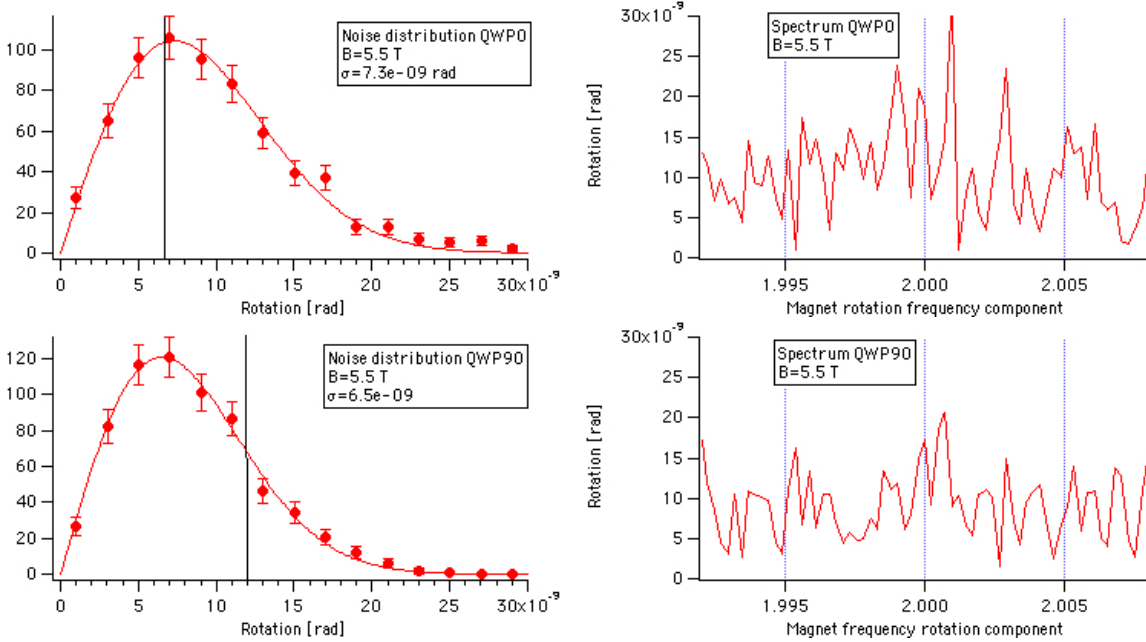

Figure 5: *Left: QWP0 and QWP90 noise distributions in the magnet rotation frequency band* $1.92\Omega_{Mag}$ *-* $2.08\Omega_{Mag}$ *for the 5.5 T rotation measurements. The vertical line indicates the resulting amplitude determined from a weighted average of 100 s long data subsets. Indicated is the value of σ for the two configurations. Right: zoom around $2\Omega_{Mag}$ of the Fourier spectrum of the entire data set showing no peak at the $2\Omega_{Mag}$. (see text)*

As can be seen in Figure 3 a peak appears at the magnet rotation frequency Ω_{Mag} when working at 5.5 T, and this is interpreted as due to a Faraday rotation in the FP cavity mirrors caused by the fringe field vertical component (see discussion above).

2. Ellipticity measurements

Also in the ellipticity column of Figure 3 no signal peaks appear at $2\Omega_{Mag}$ at 0 T, 2.3 T, and at 5.5 T. The peak at the magnet rotation frequency, Ω_{Mag}, present in the 5.5 T row can be interpreted partly as due to the mirror Faraday rotation transformed into an ellipticity by the presence of the FP cavity itself [20] and partly from beam movements on the cavity mirrors.

Again a histogram of the noise between $1.92\Omega_{Mag}$ and $2.08\Omega_{Mag}$ is shown in Figure 6 for the 2.3 T data with the vertical line indicating the value determined at $2\Omega_{Mag}$ as the weighted average of 100 s data subsets. The resulting amplitude is $9.5 \cdot 10^{-9}$. A zoom of the Fourier spectrum around $2\Omega_{Mag}$ of the data is also shown in Figure 6, at right. By using the σ obtained from the Rayleigh distribution as an estimate of the error on the measured amplitude, the value at $2\Omega_{Mag}$ is well within the 95% confidence limit. An upper limit of $\psi_{2.3} = 1.4 \cdot 10^{-8}$ at a 95 % confidence level can therefore be determined from the ellipticity data at 2.3 T.

At 5.5 T the ellipticity measurements shows a narrow peak at $2\Omega_{Mag}$. The amplitude value of the peak normalized to 5.5 T is $\psi_{5.5} = (9.7 \pm 1.3) \cdot 10^{-8}$ well above background. By considering a B^2 dependence of a possible physical signal, at 2.3 T one would have expected an ellipticity $\psi_{2.3} = 1.7 \cdot 10^{-8}$ which, given a σ of $5.6 \cdot 10^{-9}$ at 2.3 T, is excluded at a 99% confidence limit. The ellipticity peak at 5.5 T must be therefore of instrumental origin.

3. Summary of results

Table III gives the 95% confidence level background values for both rotation and ellipticity measurements. Data were taken with a typical cavity finesse of 70000, corresponding to about 45000 passes through the magnetic field zone. The total measurement time at 2.3 T field intensity was 47300 s for rotation and 65200 s for ellipticity, while at 5.5 T it was 30100 s for rotation and 3000 s for ellipticity.

No signal peaks were observed in the trasmitted intensity spectra at twice the magnet rotation frequency both in rotation and ellipticity at 2.3 T. Assuming a B^2 dependence of the previously published rotation signal ($1.7 \cdot 10^{-7}$ rad at 5.5 T with 44000 passes in the cavity [8]), one should expect to observe, at 2.3 T, a rotation peak with an amplitude of $3.6 \cdot 10^{-8}$
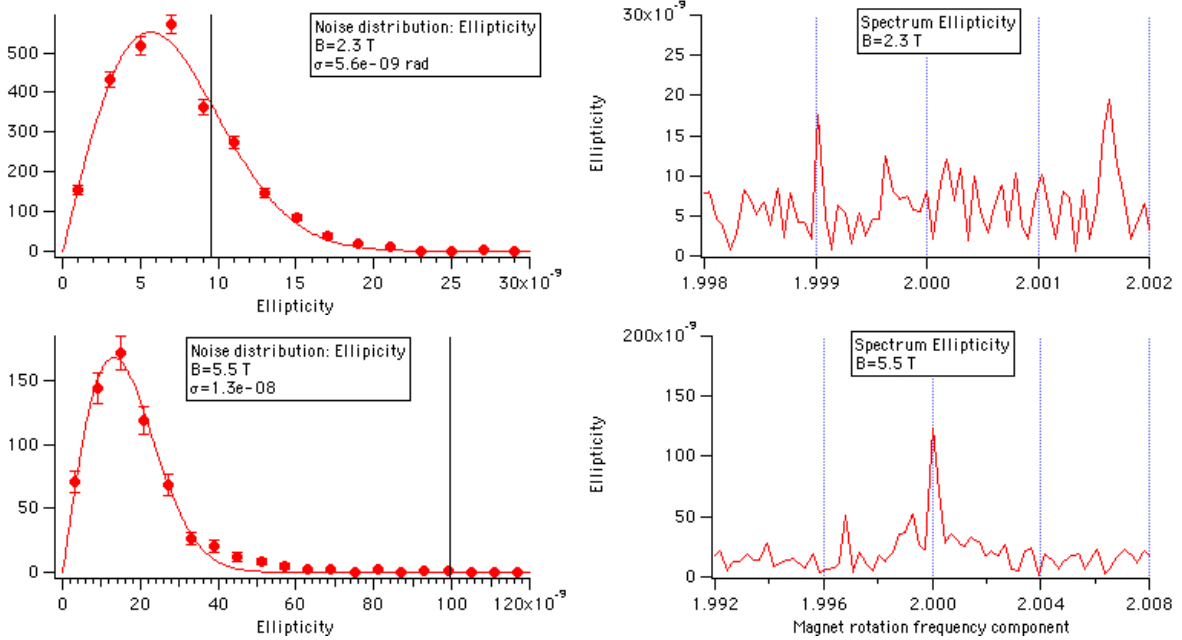
Figure 6: *Left: Noise distributions in the magnet rotation frequency band* $1.92\Omega_{Mag}$ - $2.08\Omega_{Mag}$ *for the 2.3 T (top) and 5.5 T (bottom) ellipticity measurements. The vertical line indicates the resulting amplitude determined from a weighted average of 100 s long data subsets. Indicated is the value of σ for the two field intensities. Right: zoom around $2\Omega_{Mag}$ of the Fourier spectrum of the entire data set for the two field intensities showing a peak at the $2\Omega_{Mag}$ in the case of the 5.5 T field (see text).*

Meas. Type	2.3 T	5.5 T
Rotation	$1.0 \cdot 10^{-9}$ rad	$1.2 \cdot 10^{-8}$ rad
Ellipticity	$1.4 \cdot 10^{-8}$	

Table III: Measured rotation and ellipticity backgrounds (95% c.l.) at two magnetic field intensities.

rad. Considering the value of σ for our rotation measurement at 2.3 T of $4.2 \cdot 10^{-9}$ rad such a signal is excluded with a very high confidence level. This fact immediately excludes a possible B^2 dependence of the published rotation signal. Furthermore, the absence of rotation peaks in the 5.5 T data directly contradicts the observations published in [8]. In this latter work, the relatively large dispersion of the data was treated under the hypothesis of an underlying Gaussian cause for the variability, resulting in an error estimate which, in view of the present results, was probably too small.

18

C.   Diagnostic tests on *indirect* instrumental artifacts

The vacuum measurement runs with the magnet cold and energized were followed by a series of test where we attempted to induce birefringence/rotation signals by acting externally on possible sources of indirect coupling to the light polarization. Table IV gives a summary of these tests along with the relevant comments. As a general comment, we observe here that two of the sources we investigated could potentially cause signals in both birefringence and rotation at the frequency $2\Omega_{Mag}$, namely an amplitude modulation of the SOM carrier signal and and an amplitude modulation of the laser intensity. However, when an attempt was made to stimulate these sources with local magnetic fields of the same intensity (a few Gauss) as the fringe fields generated by the superconducting magnet, no effect could be observed.

VI.   DISCUSSION AND CONCLUSIONS

The rotation measurements reported here done at a field intensity of 5.5 T indicate that the rotation signal reported in [8] was due to an instrumental artifact. Furthermore, the 2.3 T measurements, where no signal peak is visible both in rotation and in ellipticity, render improbable the hypothesis that the apparatus upgrades have themselves introduced an instrumental artifact exactly canceling the "true" previous signal, including the B^2 dependence. The limiting observed background values are

$$\alpha \leq 2.7 \cdot 10^{-13} \text{ rad/pass at } 95\% \text{ c.l. and } 5.5 \text{ T (rotation)} \tag{4}$$

$$\psi \leq 3.1 \cdot 10^{-13} \text{ 1/pass at } 95\% \text{ c.l. and } 2.3 \text{ T (ellipticity)} \tag{5}$$

The rotation limit is calculated by combining the QWP0 and QWP90 data, that is by taking the semi-difference of the weighted averages of the two data sets. These figures, using Equations 1 and 2 also set limits on the values of the observed magnetically induced birefringence and dichroism of vacuum

$$\Delta n \leq 1.1 \cdot 10^{-19} \text{ 1/pass at } 2.3 \text{ T} \tag{6}$$

$$\Delta \kappa \leq 5.4 \cdot 10^{-15} \text{ cm}^{-1} \text{ at } 5.5 \text{ T} \tag{7}$$

Table IV: List of possible sources of *indirect* coupling to the light polarization

Source	Test	Comment
Fringe-field induced modulation of the frequency-locking circuit offset (birefringence and rotation)	Directly modulate with a signal the locking circuit offset voltage	Can generate both a rotation and an ellipticity at the same frequency of the modulation
Fringe-field induced amplitude modulation of the SOM carrier signal	Modulate the amplitude the sine-wave signal exciting the SOM (typical residual modulation in actual running conditions is $\leq 10^{-3}$)	Can generate a signal at the same frequency of the modulation. Can generate a signal at the second harmonic of the modulation frequency if modulated deeply enough. Cannot be excited by a local field of the order of a few Gauss
Fringe-field induced amplitude modulation of the laser intensity	Modulate the supply current of one of the laser pump diodes (typical residual modulation in actual running conditions is $\leq 10^{-3}$)	Can generate a signal at the same frequency of the modulation. Can generate a signal at the second harmonic of the modulation frequency if modulated deeply enough. Cannot be excited by a local field of the order of a few Gauss
Fringe-field induced mechanical movements (birefringence)	Modulate by periodically moving a 40 kg inertial mass placed on the upper optical bench	Can generate a birefringence at the modulation frequency. An induced ellipticity of 1 μrad/μm was measured when mechanically moving the vacuum chambers by means of an external actuator

Furthermore, the limiting values for observed rotation and birefringence can be used to draw exclusion zones in the plane mass-inverse coupling plane for light, neutral bosons coupling to two photons [5, 6, 7]. Figure 7 shows a plot of such a parameter space. The plot contains curves calculated from the figures given in Equations 3 and 4, taking into
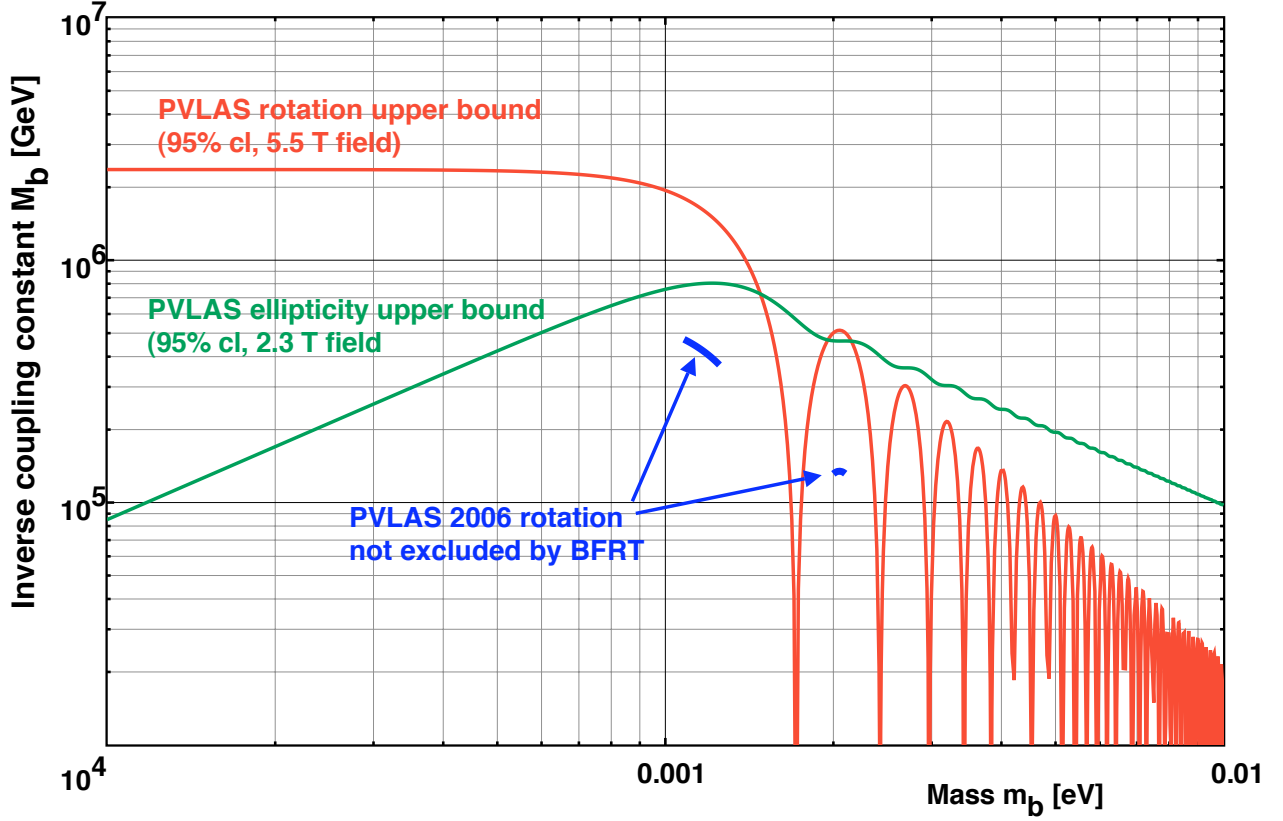
Figure 7: *Upper bounds on mass and inverse coupling constant for scalar/pseudoscalar bosons coupled to two photons. These bounds are derived from the background values reported in Table III taking into account 45000 passes in the FP cavity. Also shown are the regions calculated from the data published in [8] and compatible with the bounds reported in [9]. Our new data completely exclude our previous 2006 results [8]*

account 45000 passes in the interaction region, and shows the two portions of parameters space resulting from the previously observed rotation signal [8] and not excluded by the BFRT results [9]. Finally, the ellipticity figure can be used to set an upper bound on the

total photon-photon cross section [21], of $\sigma_{\gamma\gamma} < 6 \cdot 10^{-34}$ barn.

[1] H. Euler and B. Kochel, Naturwiss. **23** (1935) 246; W. Heisenberg and H. Euler, Z. Phys. **98** (1936) 718; V.S. Weisskopf, Mat.-Phys. Medd.-K. Dan. Vidensk. Selsk. **14** (1936) 6; J. Schwinger, Phys. Rev. **82** (1951) 664.

[2] S.L. Adler, Ann. Phys. **67** (1971) 559.

[3] E. Iacopini and E. Zavattini, Phys. Lett. B **85** (1979) 151.

[4] A.A. Anselm, Yad. Fiz. **442** (1985) 1480.

[5] L. Maiani, R. Petronzio and E. Zavattini, Phys. Lett. B **175** (1986) 359; P. Sikivie, Phys. Rev. Lett. **51** (1983) 1415; M. Gasperini, *ibid.* **59** (1987) 396.

[6] G. Raffelt and L. Stodolsky, Phys. Rev D **37** (1988) 1237.

[7] E. Massò and R. Toldrà, Phys. Rev. **52** (1995) 1755.

[8] E. Zavattini et al., Phys. Rev. Lett. **96** (2006) 110406.

[9] R. Cameron *et al.*, Phys. Rev. D **47** (1993) 3707.

[10] K. Zioutas *et al.*, Phys. Rev. Lett. **94**, 121301 (2005)

[11] See G. Raffelt hep-ph/0611350, "Lectures notes in physics", B. Beltran, M. Kuster and G. Raffelt eds., Springer (in press) and references therein.

[12] E. Massò and J. Redondo, arXiv:hep-ph/0504202.

[13] K. Van Bibber, N. R. Dagdeviren, S. E. Koonin, A. Kerman and H. N. Nelson, "An experiment to produce and detect light pseudoscalars," Phys. Rev. Lett. 59, 759 (1987).

[14] See A. Ringwald in hep-ph/0612127 and references therein.

[15] F. Brandi *et al.*, Meas. Sci. Technol. **12** (2001) 1503.

[16] See for instance M. Born and E. Wolf, *Principles of Optics*, Pergamon Press (1980), pp. 691-692.

[17] E. Iacopini, G. Stefanini and E. Zavattini, "Effects of a magnetic field on the optical properties of dielectric mirrors," Appl. Phys. A 32, 63 (1983).

[18] G. Bialolenker, E. Polacco, C. Rizzo and G. Ruoso, "First evidence for the linear magnetic birefringence of the reflecting surface of interferential mirrors," Appl. Phys. B 68, 703 (1999).

[19] C. Rizzo, A. Rizzo, D.M. Bishop, Int. Rev. Phys. Chem. 16, 81 (1997)

[20] G. Zavattini et al., "On measuring birefringences and dichroisms using Fabry-Pérot cavities,"

Appl. Phys. B 83, 571 (2006).

[21] D.A. Dicus *et al.*, Phys. Rev. D **57** (1998) 2443.